Sensorimotor neuronal learning requires cortical topography

Aamir Abbasi[1], Luc Estebanez[1], Dorian Goueytes, Henri Lassagne, Daniel E. Shulz[2] and Valérie Ego-Stengel[2,3]
Université Paris-Saclay, Centre National de la Recherche Scientifique, Paris-Saclay Institute of Neuroscience (NeuroPSI), 91190 Gif-sur-Yvette, France.
1. Equal contribution. 2. Equal contribution. 3. Corresponding author: valerie.ego-stengel@cnrs.fr

Abstract

Topographic representations of the peripheral sensory organs are a prominent feature of primary sensory areas in the cerebral cortex[1–3]. In particular, the whisker representation in the primary somatosensory cortex of rodents is composed of spatially distinct "barrel" columns, each corresponding to a different whisker on the snout[4]. Although the relationship between the sensory coding properties of neurons and their position in the barrel map has been extensively studied[5–8], the functional role of cortical maps remains unclear[9]. We hypothesize that the body map in the primary somatosensory cortex is a framework for the integration of sensory information into motor control. First, we trained head-fixed mice in a cortical closed-loop brain-machine interface task where learning necessitates the integration of sensory feedback. Second, we show that in this task a biomimetic, topographic organization of the sensory feedback is required for learning. Finally, we show that enhanced performance in the biomimetic feedback condition correlates with improved motor control. Overall our findings support the view that cortical maps are necessary for optimal cortical sensorimotor integration. They should therefore be fully considered when designing direct cortical feedback for brain-machine interfaces with clinical applications[10].

Main

We trained mice to solve a task in a cortical closed-loop brain-machine interface[11] (Fig. 1a) by controlling the activity of neurons (Fig. 1b, Extended Fig. 1) recorded in layer 5 of the primary motor cortex (vM1, Extended Fig. 2) with chronically implanted multisite silicon tetrodes. Mice had to modulate online the pooled firing rate of three selected neurons ("Master" neurons, Fig. 1c) to control the location of a virtual cursor among eight possible positions (Fig. 1d, Extended Fig. 3). When the cursor was in the "rewarded" position (4, 5 or 6, see methods), the mice could obtain water by licking a reward port. During the task, information about the current position of the virtual cursor was made available online to the mice (Emx-Cre ; Ai27 strain[12], expressing channerhodopsin in pyramidal neurons) by a continuous photoactivation of different locations of the barrel field in the primary somatosensory cortex (vS1). This feedback conveyed the current position of the cursor with a short latency (12±5 ms). The illumination pattern was made of multiple independent spots, each targeting one of the barrels that form a cortical topographic representation of the whisker hairs of the mouse snout.

Direct sensory feedback to the primary somatosensory cortex is necessary for rapid sensorimotor learning

We first showed that mice are able to rapidly learn the task when the light spots on the somatosensory cortex are spatiotemporally organized in a structured pattern that mimics physiological sequential deflection of arcs of whiskers, such as when a bar moves across the mouse snout (Fig. 1d). In this 'structured' feedback condition, over the course of 5 training sessions (one per day), the mice increased the frequency of rewards from 0.014 to 0.19 rewards/s (Example in Fig. 1e, population analysis in Fig. 1f, Mann-Whitney $U = 5$, $p < 0.001$, $n = 10$ mice). In

contrast, in the absence of feedback, the mice failed to increase the frequency of reward despite the same amount of training (0.025 vs 0.022 rewards/s, Mann-Whitney U = 31, p = 0.48, n = 8 mice, Fig. 1f).

In the structured feedback condition, the increase in reward frequency was accompanied by an increased proportion of licks that were rewarded (Fig. 1g, Mann-Whitney U = 1, p < 0.001), indicating that the mice did not simply increase the licking frequency irrespective of the cursor position in order to solve the task.

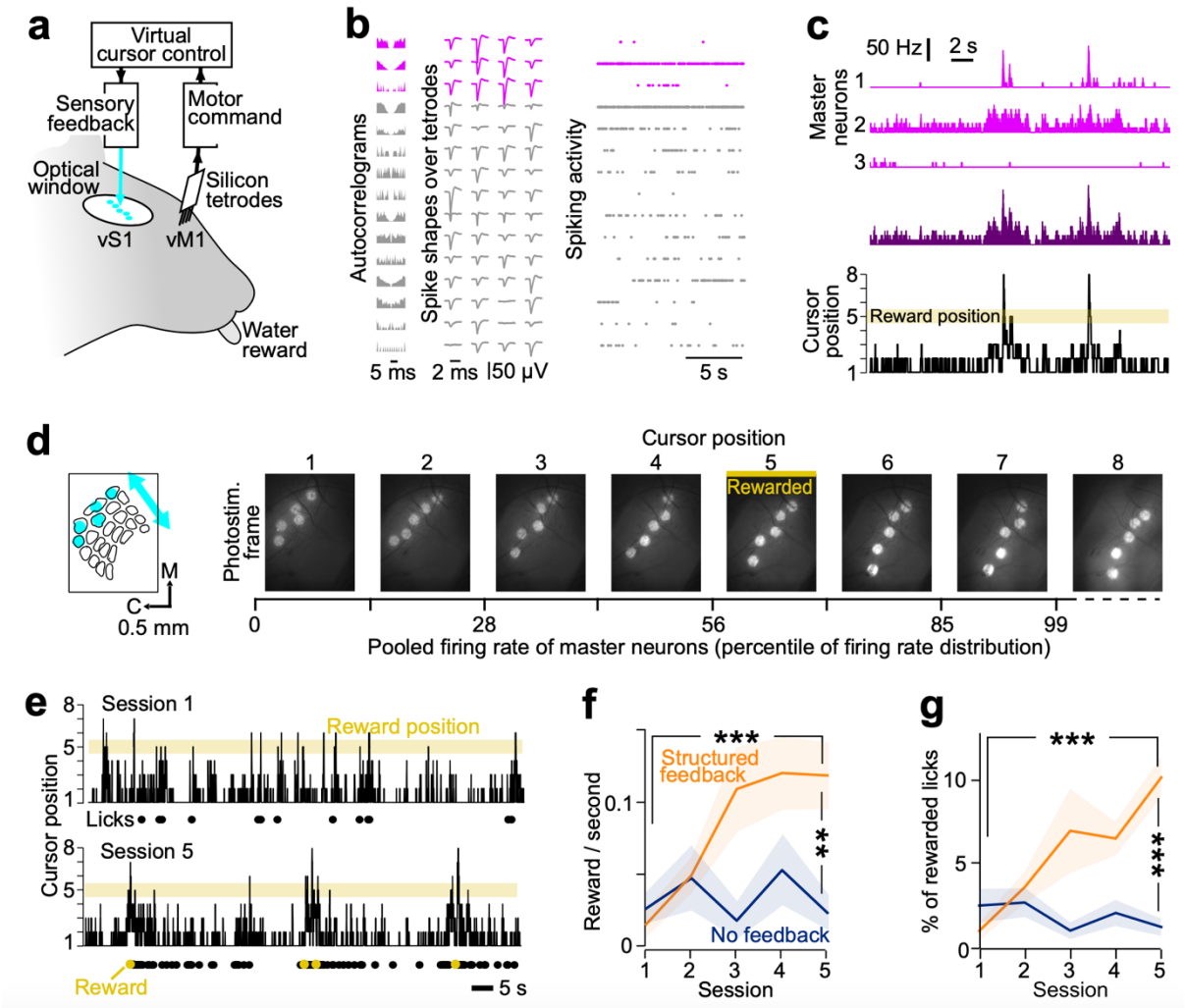

Fig. 1 | Sensory feedback to the barrel cortex enables learning of a brain-machine interface task. **a**, Closed-loop setup combining chronic extracellular readout in vM1 and optogenetic feedback that targets the barrels in vS1. **b**, Tetrode recordings of baseline activity in vM1. Purple: Master neurons that are selected to control a virtual cursor. Gray: additional simultaneously recorded neighboring neurons. **c**, Peristimulus time histogram of the 3 Master neurons (Purple). Dark purple: sum of the activity of the Master neurons, which is translated into the position of the virtual cursor (black) that must be in position 5 to obtain a reward by licking. **d**, Bar-like biomimetic photoactivation of the S1 barrels. Left: schematic of the first photostimulation frame. C: caudal, M: medial. Right: Snapshots of the cortical surface illustrating biomimetic photostimulation frames for each cursor position (structured feedback). When the cursor is in position 5, licks are rewarded. **e**, Example cursor position and licking time course during first and last training sessions using the structured feedback shown in (**d**). **f**, Frequency of the rewards during learning with structured feedback (orange, 10 mice) versus no feedback frames (blue, 8 mice). **g**, Proportion of rewarded licks (including all licks even during bursts). **: p < 0.01. ***: p < 0.001, non-parametric Mann-Whitney tests. Light backgrounds: +/- standard error of the mean (SEM).

The sensory feedback has to respect biomimetic spatiotemporal patterns to be effective

The application of optogenetic feedback to the barrel field of the somatosensory cortex was required for learning the task over 5 training sessions. However, it was unclear if any arbitrary feedback with the same informational content as the structured one would suffice for improving task performance. Or if, alternatively, the feedback mimicking a topographical, biologically plausible sequence of whisker stimulations could make it easier to integrate the information into the sensorimotor loop. To test this, we trained the same mice in an additional protocol where the feedback carried the same information about cursor position, but where the biomimetic spatial structure was disrupted using a permutation of barrel identities (Fig. 2a, 'destructured' feedback, 8 mice). In this condition, the mouse failed to learn the task, both in terms of reward rate (Fig. 2b, Mann-Whitney $U = 5$, $p = 0.095$) and proportion of rewarded licks (Fig. 2c, Mann-Whitney $U = 28$, $p = 0.36$).

Since the training order might have had an impact on the success of the structured feedback and the failure to perform the task in the two other conditions, we trained two sets of three mice with the three protocols, following two possible orders (A or B, Fig. 2d). Irrespective of the protocol order, significant learning was only observed in the structured feedback condition (Mann-Whitney $U = 0$, $p = 0.04$). We conclude that the training order does not impact noticeably the learning process.

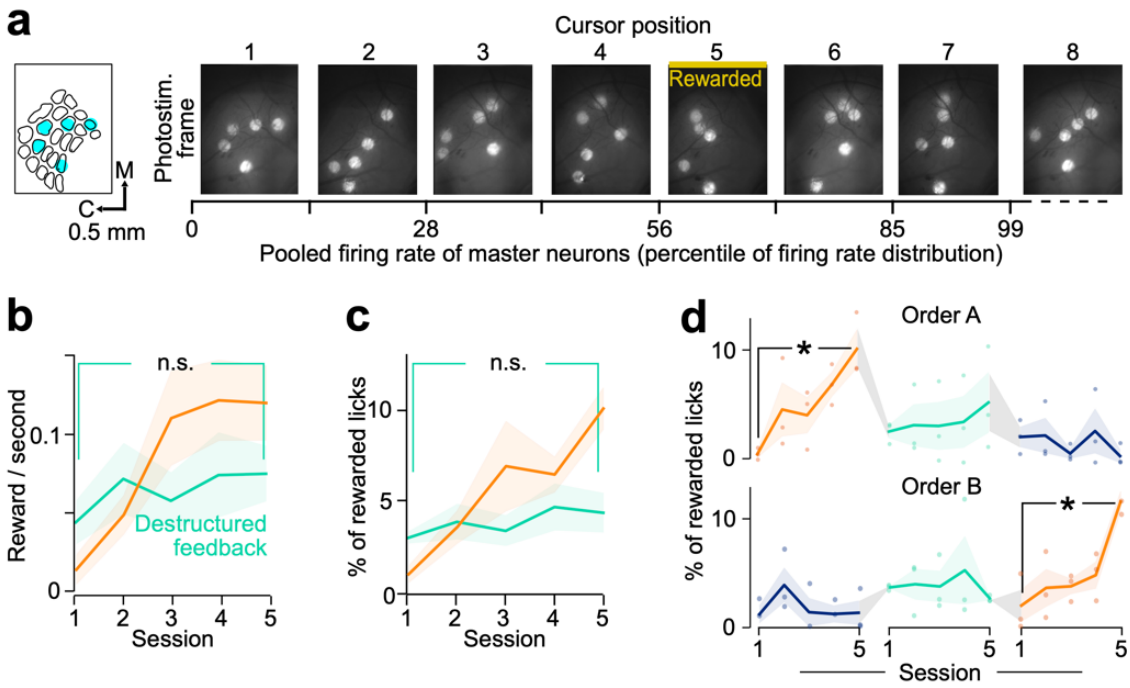

Fig. 2 | Learning relies on biomimetic feedback. a, Left: schematic of the first destructured photostimulation frame. Right: snapshots of the cortical surface illustrating the destructured photostimulation frames for each cursor position. **b**, Mean reward frequency across training sessions with structured (orange, 10 mice) and destructured (green, 8 mice) feedback. **c**, Same as **b** for percentage of rewarded licks. **d**, Learning for two different orders of task training with the three protocols: structured (orange), destructured (green) and no feedback (blue). *: $p < 0.05$. Mann-Whitney non-parametric tests. Individual data points are overlaid. Light backgrounds: +/- SEM.

Open-loop sensory-guided behavior does not require biomimetic stimulation

The drop in performance between learning in the structured and destructured feedback conditions may result from altered integration of the sensory information at different stages of the sensorimotor loop. For example, it might result from impaired processing of the optogenetic inputs in the barrel cortex under the destructured feedback condition. If it were the case, mice should fail to use destructured cortical sensory inputs even in the context of a purely sensory task, devoid of a motor control component. To test this hypothesis, we carried an additional series of experiments in three mice that were exposed to two playback sessions following training with both the destructured and structured conditions (Fig. 3a). In contrast with the standard closed-loop training, during the playback sessions the ongoing activity of motor cortex neurons was not responsible for controlling the cursor, and indeed there was no increase in their firing rate before rewards (Fig. 3b top). Instead, the mice were exposed to sequences of optogenetic stimulation corresponding to cursor positions that they had experienced in a previous structured feedback session. To obtain rewards, the mice still had to lick when the cursor was in position 5 (Fig. 3b bottom).

In this playback condition, the reward rate dropped (Fig. 3c, top) but the proportion of rewarded licks remained elevated (Fig. 3c, bottom). Moreover, the performance observed in the playback condition using destructured frames was significantly higher than in the closed-loop destructured feedback condition (compare the first and the last points of both graphs in Fig. 3c). These observations show that even with destructured frames, the integration of optogenetic inputs took place, to drive sensory-guided behavior. This suggests that in the destructured closed-loop task, the production of appropriate motor commands was impaired at a later stage of the sensorimotor loop, beyond the somatosensory cortex.

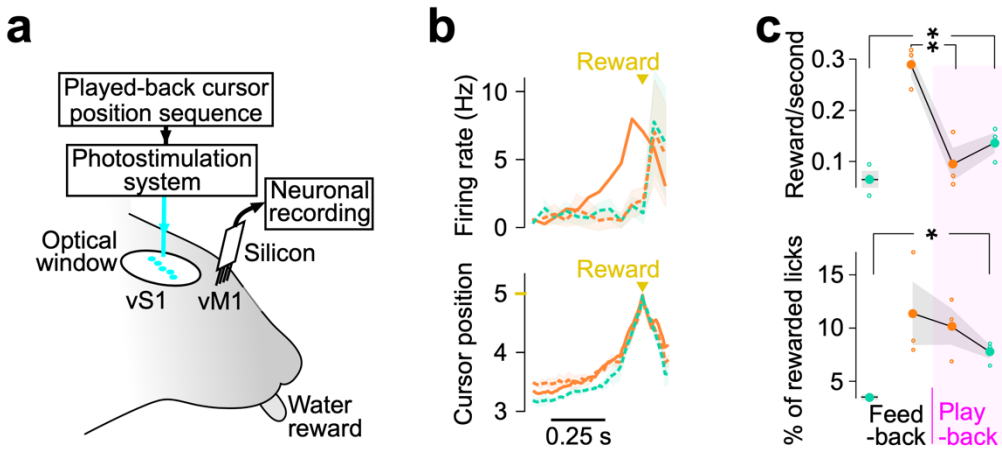

Fig. 3 | Playback performance holds across photostimulation conditions. a, Principle of playback experiments. **b**, Average firing rate (top) and average cursor position (bottom) around reward time. Continuous orange line: last session of structured closed-loop feedback. Dashed orange line: playback of photostimulation from the last structured feedback session. Dashed green line: playback of the same session, using destructured instead of structured frames. **c**, Frequency of rewards (top) and proportion of rewarded licks (bottom) for three mice tested across 4 sessions, from left to right: last destructured closed-loop feedback session; last structured closed-loop feedback session; playback session with structured frames; playback session with destructured frames. Sessions connected by a line are consecutive. *: Mann-Whitney $p < 0.05$. Gray background: +/- SEM.

The spatial structure of the sensory feedback impacts motor control

As shown above, the structured and destructured feedbacks were not equally efficient in driving motor learning beyond the somatosensory cortex. The motor cortex activity and the resulting motor control of the virtual cursor could be particularly impacted by the topographical organization of the feedback. Consistent with this hypothesis, we observed a significant increase of the standard deviation of the firing rate of Master neurons exclusively in the structured feedback condition (which was not present in simultaneously recorded 'Neighbor' neurons, Extended Fig. 4a,b). This resulted in a significant increase of the time spent by the cursor in the rewarded position, from 2.4% in the first session, to 3.9% in the fifth (Mann-Whitney U = 10, p = 0.037, n = 6 mice). This was not true for destructured stimulations (1.1% to 1.7% from first to last session, Mann-Whitney U = 10, p = 0.13, n = 6 mice).

This increase in time spent in the rewarded position during the structured protocol could result either from a higher variability of mean firing rate randomly distributed across time, or from an improved neuronal control of the cursor. To test this, we focused at a finer time scale on cursor movements that took place just before a rewarded lick (Fig. 4a). We found that in the structured feedback condition, the cursor position before reward was significantly closer to the reward position after 5 than after 3 sessions of learning (Fig. 4a), and we observed a sharp increase of the duration spent in the reward position (from 139 ms to 246 ms in a 2 s window around reward time, Fig. 4b).

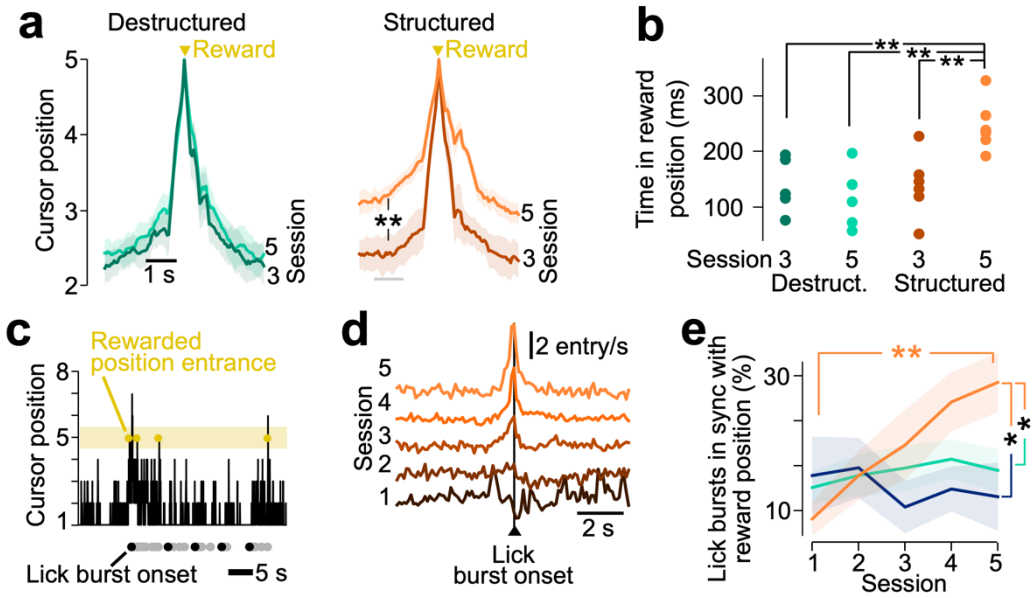

Fig. 4 | Learning with structured feedback shapes the cursor dynamics. a, Mean trajectory of the cursor position aligned to the reward time for the 6 mice where position 5 was rewarded. Left: destructured condition. Dark green: session 3. Light green: session 5. Right: same for structured feedback. Test: comparison of the average firing rates in the gray 1 s window, between structured sessions 3 and 5. We compared session 5 to session 3 due to the lack of rewards in sessions 1 and 2. **b**, Average time spent by individual mice in the rewarded cursor position. **c**, Example behavior. Gray dots: licks. Black: onset of lick bursts. Yellow dots: time of entrance in the rewarded cursor position. **d**, Population average histogram of the times of entrance in the rewarded cursor position around the onset of lick bursts with structured feedback, across five training sessions. **e**, Percentage of licks bursts that are synchronous (within ±100 ms) with onset of the rewarded feedback frame. Orange: structured; Green: destructured; Blue: no feedback. *: Mann-Whitney $p < 0.05$. **: $p < 0.01$. ***: $p < 0.001$. Light backgrounds: +/- SEM.

Average licking statistics also evolved, with a significantly increased variability during structured learning (Extended Fig. 4c,d). We wondered if – in combination with the cursor learning – this led to a better synchronization of licks with the reward position (example illustrated in Fig. 4c). We computed time histograms of the onsets of entrance in the rewarded position, aligned on the onset of lick bursts (Fig. 4d). We quantified the peaks in these histograms by measuring the proportion of all lick burst onsets that occurred in synchrony (+/-100 ms) with an entrance in the rewarded position (Fig. 4e). It increased significantly across sessions in the structured (Mann-Whitney $U = 11$, $p = 0.002$, $n = 10$) but not in the destructured (Mann-Whitney $U = 27$, $p = 0.32$, $n = 8$) and the no-feedback conditions (Mann-Whitney $U = 23$, $p = 0.19$, $n = 8$). This increased correlation was specific to the licking activity, as we found no relationship between other body movements (whisking, paw movement, ear movements) and neuronal activity (Extended Fig. 5).

These results confirm that mice learned to coordinate their motor actions only when the sensory feedback was topographically organized.

Conclusion

Using a closed-loop sensorimotor brain-machine interface approach, we have shown that a biomimetic spatiotemporal organization of the sensory feedback is required for efficient sensorimotor integration. Learning with the biomimetic structured feedback was associated with improved motor control of the virtual cursor. Combined with accurate lick timing, this resulted in a significant increase in the overall behavioral performance of the mice. By directly demonstrating that the spatiotemporal structure of inputs to a cortical map can have a causal impact on task learning and behavioral performance, these findings indicate that maps are a fundamental building block of cortical processing[9,13,14].

Our data also constitute a direct observation that the predictability of upcoming sensory information – which is present only in the structured feedback in our experiments – is important for sensorimotor integration[15]. Finally, these results emphasize that a biomimetic design of cortical feedback signals has to be considered for optimizing cortical brain-machine interfaces in humans[10].

Acknowledgements

We thank Isabelle Férézou for advice on experimental design and analysis; Daniel Feldman, Suliann Ben Hamed, Karim Benchenane, Boris Barbour, German Sumbre and Evan Harrell for comments on an earlier version of the manuscript. Aurélie Daret and Guillaume Hucher provided experimental support. CNRS, ANR Neurowhisk, Lidex NeuroSaclay, Idex Brainscopes and iCODE, FRM (Equipe FRM DEQ20170336761) and FRC (AAP 2018) provided funding.

Data Availability statement

All data will be available upon request to the corresponding author.

Author contribution statements

D.E.S and V.S. initiated the project. D.E.S, L.E and V.S designed the experiments and analysis; A.A. performed the experiments, with support from L.E., H.L. and D.G.; L.E and A.A. analyzed the data with support from H.L.; L.E., V.S. and D.E.S wrote the manuscript with input from all authors.

Author identification (ORCID IDs)

Aamir Abbasi: 0000-0002-7330-7498

Luc Estebanez: 0000-0001-6253-7637

Dorian Goueytes : 0000-0002-0836-5333

Henri Lassagne : 0000-0002-0583-9900

Daniel E. Shulz : 0000-0002-9571-4588

Valérie Ego-Stengel : 0000-0002-9099-9051

Bibliography

1. Penfield, W. & Boldrey, E. Somatic motor and sensory representation in the cerebral cortex of man as studied by electrical stimulation. *Brain* **60**, 389–443 (1937).

2. Adrian, E. D. Afferent discharges to the cerebral cortex from peripheral sense organs. *J. Physiol.* **100**, 159–191 (1941).

3. Hubel, D. H. & Wiesel, T. N. Receptive fields, binocular interaction and functional architecture in the cat's visual cortex. *J. Physiol.* **160**, 106–154 (1962).

4. Woolsey, T. A. & Van der Loos, H. The structural organization of layer IV in the somatosensory region (SI) of mouse cerebral cortex: the description of a cortical field composed of discrete cytoarchitectonic units. *Brain Res.* **17**, 205–242 (1970).

5. Simons, D. J. Response properties of vibrissa units in rat SI somatosensory neocortex. *J. Neurophysiol.* **41**, 798–820 (1978).

6. Andermann, M. L. & Moore, C. I. A somatotopic map of vibrissa motion direction within a barrel column. *Nat. Neurosci.* **9**, 543–551 (2006).

7. Kremer, Y., Leger, J.-F., Goodman, D., Brette, R. & Bourdieu, L. Late Emergence of the Vibrissa Direction Selectivity Map in the Rat Barrel Cortex. *J. Neurosci.* **31**, 10689–10700 (2011).

8. Estebanez, L., Bertherat, J., Shulz, D. E., Bourdieu, L. & Léger, J.-F. A radial map of multi-whisker correlation selectivity in the rat barrel cortex. *Nat. Commun.* **7**, 13528 (2016).

9. Kaas, J. H. Topographic Maps are Fundamental to Sensory Processing. *Brain Res. Bull.* **44**, 107–112 (1997).

10. Bensmaia, S. J. & Miller, L. E. Restoring sensorimotor function through intracortical interfaces: progress and looming challenges. *Nat. Rev. Neurosci.* **15**, 313–325 (2014).

11. Abbasi, A., Goueytes, D., Shulz, D. E., Ego-Stengel, V. & Estebanez, L. A fast intracortical brain–machine interface with patterned optogenetic feedback. *J. Neural Eng.* **15**, 046011 (2018).

12. Madisen, L. *et al.* A toolbox of Cre-dependent optogenetic transgenic mice for light-induced activation and silencing. *Nat. Neurosci.* **15**, 793–802 (2012).

13. Sur, M., Garraghty, P. E. & Roe, A. W. Experimentally Induced Visual Projections into Auditory Thalamus and Cortex. *Sci. New Ser.* **242**, 1437–1441 (1988).

14. Horton, J. C. & Adams, D. L. The cortical column: a structure without a function. *Philos. Trans. R. Soc. B Biol. Sci.* **360**, 837–862 (2005).

15. Brecht, M. The Body Model Theory of Somatosensory Cortex. *Neuron* **94**, 985–992 (2017).

16. Okun, M., Lak, A., Carandini, M. & Harris, K. D. Long Term Recordings with Immobile Silicon Probes in the Mouse Cortex. *PLOS ONE* **11**, e0151180 (2016).

17. Ceballo, S., Piwkowska, Z., Bourg, J., Daret, A. & Bathellier, B. Targeted Cortical Manipulation of Auditory Perception. *Neuron*, in press.

18. Knutsen, P. M., Mateo, C. & Kleinfeld, D. Precision mapping of the vibrissa representation within murine primary somatosensory cortex. *Philos. Trans. R. Soc. B Biol. Sci.* **371**, 20150351 (2016).

19. Yger, P. *et al.* A spike sorting toolbox for up to thousands of electrodes validated with ground truth recordings in vitro and in vivo. *eLife* **7**, e34518 (2018).

20. Mathis, A. *et al.* DeepLabCut: markerless pose estimation of user-defined body parts with deep learning. *Nat. Neurosci.* **21**, 1281–1289 (2018).

Methods

Methodological details of the closed-loop interface setup can be found in a previous publication[11].

Mouse preparation. All animal experiments were performed according to European and French law as well as CNRS guidelines and was approved by the French ministry for research (ethical committee 59, authorization 858-2015060516116339v5). The data was obtained from 12 adult (6-10 weeks old) Emx1-Cre;Ai27 mice. All surgeries were performed under isoflurane anesthesia (1%–4% Isoflurane depending on mouse state, assessed by breathing rate and response to tail pinch), in 100% air. For each mouse, during a first surgery, a 5 mm glass optical window was implanted over the primary somatosensory cortex (vS1, P-1.5 mm and L-3.3 mm, from bregma) and a head-fixation bar was implanted on the contralateral side of the skull. Eight days later, intrinsic imaging was performed during mechanical deflection of at least 3 individual whiskers to locate a subset of barrels in the barrel cortex. In the following days, a second surgery was performed to chronically implant[16] a Neuronexus 32 channel silicon probe (A1x32Poly35mm25s 177A32, Neuronexus, USA) in the whisker motor cortex (vM1, A1.5 mm L0.6 mm from bregma, electrode recording sites 650 – 800 μm deep in cortex).

Neuronal recordings. Following the surgery, the mice were monitored during 5 days to ensure stability of the shape and amplitude of the units isolated by the online spike sorting (Blackrock microsystems, USA). Clusters corresponding to well-defined single units (consistent spike shape and adequate autocorrelogram, Fig. 1b) were manually selected within the tetrode spike amplitude space. This manual selection was updated before each session. This ensured that we maintained unit separation while keeping track as much as possible of the same units across sessions (Extended Fig. 1). Once units were selected, the training session was initialized and individual spikes were sorted according to the pre-defined clustering. At the start of the training sessions, we recorded a median of 25.5 neurons (IQR = 5.25 neurons, n = 10 mice). After 17 days (average last training session) we recorded a median of 25 neurons (IQR = 16 neurons, n = 10 mice).

Brain-machine interfacing. Among the recorded units of each mouse/session, a set of 3 putative pyramidal neurons – the Master neurons – were selected by the operator. Their summed activity was then convolved with a 100 ms box kernel and its value determined a virtual cursor position. The mice were required to control the position of the cursor to solve the task. To do so, the values of the summed firing rate of the Master neurons were recorded during the first 3 minutes that preceded the start of the session. A threshold was set at the 99th percentile of theses baseline activity values, and the activity space from 0 up to this threshold was split in 7 equal positions, with an extra 8th position for values above the 99th percentile threshold. For six mice, the 5th position was systematically rewarded, which means that whenever the cursor was inside that position and the mouse simultaneously licked, it obtained a 5 μL water drop (Extended Fig. 3). If one neuron was lost during the training, the active Neighbor neuron with the largest spikes shape was enrolled to replace it. If no additional Neighbor neuron was available, the experiment kept going with only two Master neurons. For the other 6 mice, either the 6th or the 4th position was rewarded. These mice were not included in the analysis of cursor position (figure 4).

Optogenetic photostimulation. Each cursor position was associated with a specific feedback pattern that was projected onto the barrel cortex of the mice using a Digital Light Processing module (DLP, Vialux V-7001, Germany). The DLP contained a 1024 x 768 pixels Texas Instruments micro-mirror chip, which was illuminated by a high-power 462 nm blue LED. The image stream generated by the device was focused onto the cortical optical window using a tandem-lens macroscope[17]. This device was used to send homogeneous light spots, 200 μm in diameter, centered onto the barrel locations for the mouse strain/age that we used[18]. A set of reference barrels (at least 3) that were located during the mouse preparation via intrinsic imaging were used to align a standard barrel map[18]. We used three different sets of feedback frames to obtain the 3 conditions we tested: structured (Fig. 1d), destructured stimulations (Fig. 2a), and finally a condition where no photostimulation was displayed (no feedback).

Behavioral training. Mice were first habituated to head-fixation (1 session). Then, they were water deprived and learned to lick for water from a reward tube in front of their mouth (1-2 sessions). Finally, the mice were trained on the 3 different feedback conditions for 5 sessions a week (1 session/day). Training sessions lasted for 30 minutes each. Mice were checked daily for weight and extra water/food intake was provided as needed to stabilize the weight at 80% of their initial value.

Offline spike sorting. Offline extraction of neuronal activity was performed using SpyKING CIRCUS[19]. We manually confirmed that each online sorted Master unit did correspond to specific offline-sorted units. All additional, non-Master offline-sorted units were labeled as Neighbor units.

Data Analysis. All tests are non-parametric, two-sided Mann-Whitney tests. In figure 1 to 3 all licks are taken into account. In Figure 4e, lick bursts are defined as series of licks where the inter-lick interval is smaller than 200 ms.

Histology. After the experiment, mice were deeply anaesthetized with isoflurane (4-5%) and pentobarbital then exsanguinated and perfused with 4 % paraformaldehyde (PFA). The brains were removed and stored overnight in 4% PFA. The brains were then transferred to a solution of PBS for at least 24 hours before 50 μm slices in the coronal plane were cut and stained using cytochrome C oxidase. The location and depth of the silicon probe in the brain were traced by looking at the fluorescent dye DiI that was deposited on the electrodes prior to their implantation.

ICMS experiments. To confirm that the electrodes were located in a motor cortical area, we performed intracortical microstimulation (ICMS) at the end of the behavior sessions (n = 3 mice). We sent bipolar current pulses (amplitude 21 μA/channel, duration 1.4 s, frequency 60 Hz) through the 32-channel Neuronexus silicon probe implanted in vM1, in awake head-fixed animals. The contralateral whiskers were imaged using a high-speed videography (camera – Baumer HXc-20, lens – 6 mm, F/1.4) at 300 frames per seconds for a duration of 9 s. A single trial consisted of 5 s pre-ICMS videography, followed by 1.4 s during ICMS stimulation and finally 2.6 s post-ICMS. This procedure was repeated 14 times during a single session of ICMS experiment, with a 1 s inter-trial. In the ICMS videos, a central whisker was identified amongst all the whiskers in the field of view, and tracked using automated video tracking software DeepLabCut[20]. The amplitude of ICMS-evoked whisker movement was defined as the mean whisker angle during the first 1 s of stimulation versus the 1s immediately before. Latency of whisker movement was measured at the first frame with significant whisker movement amplitude (2 standard deviations above the mean).

Mouse imaging experiments. We tracked mice body movements at 100 frames per second during sessions where the mouse was head-fixed but was not involved in an active behavior. During these experiments the activity of the M1 neurons was recorded. There was no visible correlation between the activity of Master neurons and the movements of whiskers, ear or forepaw (Extended Fig. 5).

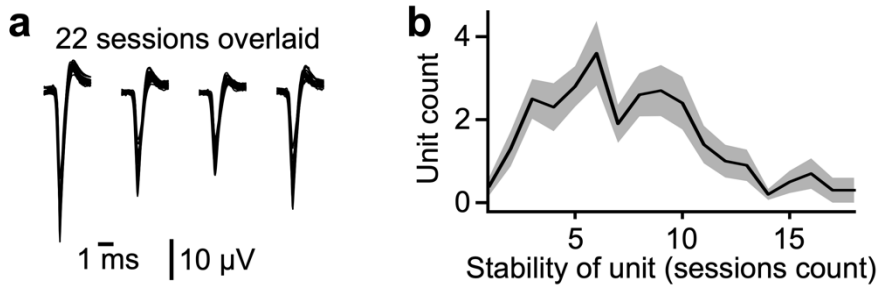

Extended Fig. 1 | Stability of the recorded neurons. a, Tetrode spike shape of one neuron, overlaid over 22 sessions (1 session/day). **b**, Average distribution of the number of sessions where the same unit could be identified in the recording, for all 12 mice included in the dataset. Gray background: standard error of the mean. Total amount of recorded sessions ranged from 17 up to 34.

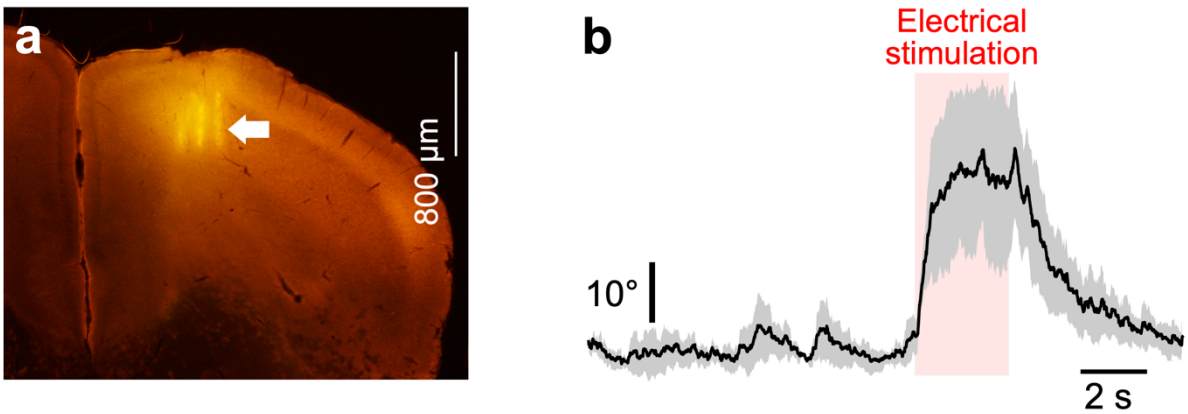

Extended Fig. 2 | Localization of the implanted silicon probes in whisker vM1. a, Coronal slice (50 µm thick) of a mouse brain, stained with Cytochrome oxidase, confirms the location of the silicon tetrode array in (white arrow). DiI coating of the shanks prior to insertion resulted in fluorescent lines indicative of the location of single shanks (yellow tracks). **b**, The amplitude of angular movements of the contralateral whiskers evoked by ICMS stimulation through the silicon probe (average of 3 mice) confirms that the electrode was located in vM1. Light background: standard error of the mean.

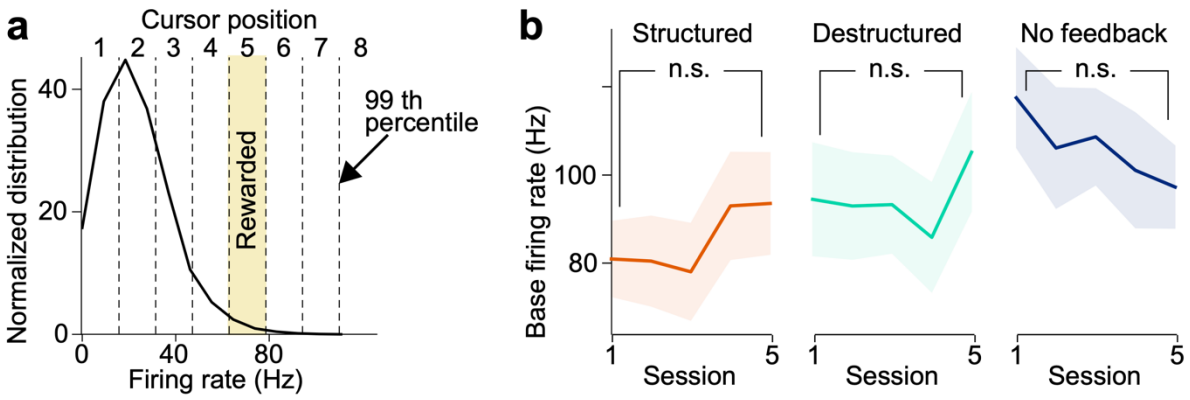

Extended Fig. 3 | Definition of the firing rate limits of the positions of the cursor. a, Example distribution of the firing rate during the 3 min baseline at the start of a session. Positions correspond to equal firing rate intervals. Position 1 starts at 0 Hz firing rate. The transition between cursor positions 7 and 8 is set at the 99th percentile of the firing rate distribution. **b**, The 99th percentile of the firing rate (averaged across mice) did not significantly evolve over training sessions (n.s.: Mann-Whitney p value > 0.05). Light background: +/- SEM.

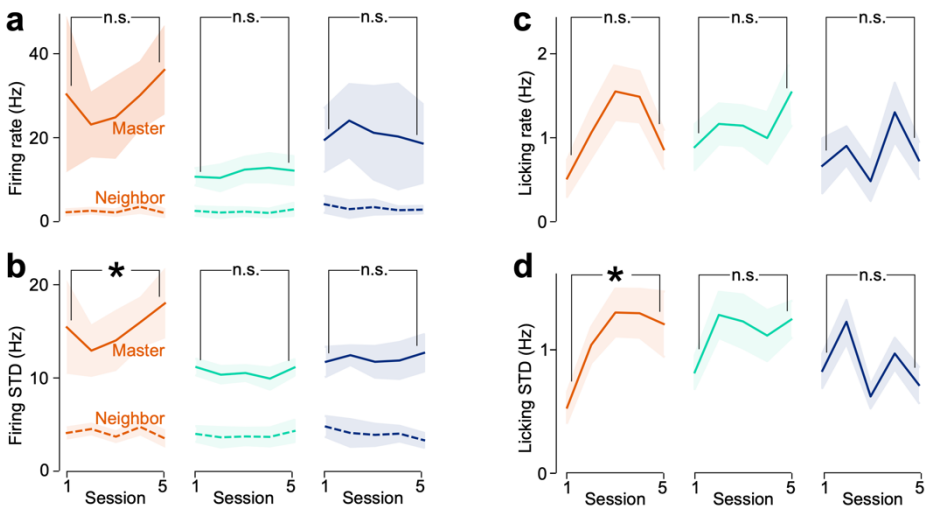

Extended Fig. 4 | Firing statistics of Master and Neighbor neurons, and licking statistics, during closed-loop learning. **a**, Average firing rate across all mice of Master (continuous line) and Neighbor neurons (dashed line) over 5 training sessions, during the structured (orange), destructured (green) and no-feedback (blue) conditions. Light background: +/- SEM. **b**, Same as **a** for the standard deviation of the firing rate (measured over 1 s windows). **c**, Average licking rate over sessions. **d**, Average standard deviation of the licking rate (measured over 1 s windows). All tests: Mann-Whitney. *: p < 0.05.

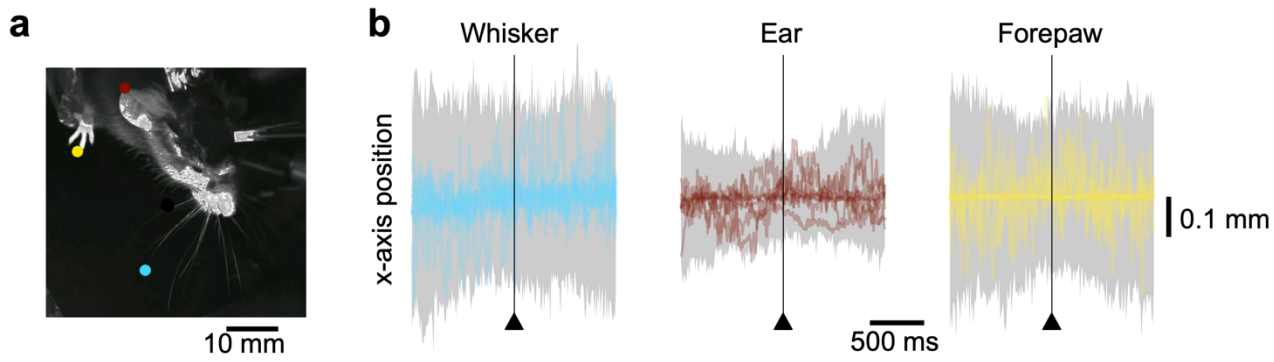

Extended Fig. 5 | Relationship of Master neurons activity with body movements during a spontaneous behavior session after the training sessions. **a,** Tracked body parts positions, including a whisker (blue), the right forepaw (yellow) and the right ear (red). **b**, Individual traces correspond to the average spike-triggered movement of the body parts selected in the picture in **a**, for each individual Master neurons of 3 mice, during a session of spontaneous behavior. Gray background: bootstrap-based 1% significance threshold for the spike-triggered analysis of the movements. Left: Whisker movements. Middle: Ear movements. Right: Forepaw movement.